Bioxidant corrosion behaviour of CoNiCrAlY coated IN738 at 1100 °C

H. Chen[a,*], X. Hou[b], J. He[c] and H. Guo[c,*]

[a]Department of Mechanical, Materials and Manufacturing Engineering, Faculty of Science and Engineering, University of Nottingham Ningbo China, Ningbo 315100, China

[b]Advanced Materials Research Group, Faculty of Engineering, University of Nottingham, University Park, Nottingham NG7 2RD, UK

[c]School of Materials Science and Engineering, Beihang University (BUAA), No. 37 Xueyuan Road, Beijing, China

Abstract

This paper investigates the bioxidant corrosion behaviour of CoNiCrAlY coated IN738 at 1100 °C. Free-standing CoNiCrAlY coatings and CoNiCrAlY coated IN738 were isothermally oxidised in air at 1100 °C for periods up to 100 h. It is found that the bioxidant corrosion occurred in the coated IN738 samples, in which the β phases in the CoNiCrAlY coating were significantly consumed by internal oxidation and internal nitridation. Aluminium nitrides and titanium nitrides were found to exist in the CoNiCrAlY coating after bioxidant corrosion. The internal nitridation is likely to occur when no protectives oxides can form at the coating surface.

Keywords: CoNiCrAlY; IN738; Bioxidant corrosion; Internal nitridation; β-phase depletion

*Corresponding Authors.

E-mail address: Hao.Chen@nottingham.edu.cn, guo.hongbo@buaa.edu.cn

1. Introduction

MCrAlY (M = Fe, Co and/or Ni) coatings are widely used for oxidation-corrosion protection of high temperature components due to their excellent oxidation and corrosion resistance [1-8]. It is generally recognised that the protective effect of MCrAlY coatings is achieved by forming a dense and stable alumina scale at the coating surface in elevated temperature environments [9-16]. Depending on the compositions, MCrAlYs usually exhibit γ+β or γ+γ'+β multiphase structures. Work concerned on the oxide growth, β-phase depletion and interdiffusion in MCrAlY coating systems have been extensively reported, ranging from experimental studies to numerical simulations [17-33]. But in reality the oxidation and corrosion behaviour of MCrAlY coatings varies with many factors, such as exposure conditions, heat treatment history, microstructural characteristics and coating/substrate systems [34-46]. It is reported that the oxide growth and β-phase depletion are largely affected by the oxidation temperatures [47]. It is shown that the oxidation rate appears rather slow below 800 °C but it is significantly accelerated when the temperature is above 1000 °C [48]. It is also noticed that the oxide growth and spallation is closely related to the surface morphology and heat treatment history of the coating [49-52]. To facilitate the growth of the protective alumina scale, it has been demonstrated that an initial heat treatment can suppress the spinel oxides formation and allow the alumina scale to growth [39]. Furthermore, it has been found that the substrate can influence the oxidation behaviour of MCrAlY coatings and early spallation of the protective oxides might occur [53-55]. This is likely to alter the oxidation mechanism of MCrAlY coatings from external oxidation to the highly undesirable internal oxidation and internal nitridation, which is also termed bioxidant corrosion.

A few studies have reported the phenomenon of bioxidant corrosion in MCrAlYs and Ni-based superalloy systems [56-62]. Early work by Lit et al. [56] and Krupp et al. [57, 58] has shown that the selective oxidation and internal nitridation can occur in Ni-based superalloys at high temperatures. They have found that the AlN and TiN are likely to form underneath the

oxide scale during high temperature exposures. Han et al. have examined the kinetics of internal oxidation and nitridation in Ni-Cr-Al alloys, in which an internal oxidation zone immediately beneath the surface, consisting of Al_2O_3 and Cr_2O_3, and a wide internal nitridation zone, composing of AlN and Cr_2N, are reported [59]. Similar findings in FeCrAlY alloys have also been reported by Bennett et al. [60]. More recently, the bioxidant corrosion behaviour in MCrAlY coated Ni-based superalloys has also been reported [61, 62]. It is found that the formation of AlN and TiN occurs near the coating/substrate interface and the Ti content in the substrate plays a dominant role in nitrides formation and subsequent bioxidation corrosion. These studies indicate a potential limitation of using MCrAlYs on high Ti-content Ni-based superalloys. However, due to the limited studies available on the bioxidation corrosion of MCrAlY systems, the mechanisms of thermodynamically induced internal nitridation have not been well understood yet.

Therefore, considering the significance of bioxidant corrosion on the durability of MCrAlY coating systems, the aim of this study is to investigate the bioxidant corrosion mechanisms of MCrAlY coated IN738, specifically on the microstructural evolution of nitrides formation in the system. Ni-based IN738 superalloy substrate is used here since it has a relatively high Ti content (3.4 wt%). Since the Co-based MCrAlY was reported to have good corrosion and oxidation resistance [2], free-standing Co-based MCrAlY (CoNiCrAlY) coatings are employed as the reference samples in order to the compare and contrast the oxidation behaviour of MCrAlY coated IN738. The isothermal oxidation behaviour of the above coating samples were examined at 1100 °C for times up to 100 h. The thermodynamic software, Thermo-Calc, is used to evaluate the thermodynamic properties of the oxides and nitrides in the TCNI8 thermodynamic database. The work reported here is aiming at revealing the mechanisms of bioxidant corrosion in MCrAlY coated IN738 at elevated temperatures.

2. Experimental procedure

2.1. Materials

A commercially available Co-based MCrAlY (CoNiCrAlY) powder (Praxair CO-210-24, Co-31.7%Ni-20.8%Cr-8.1Al%-0.5%Y in wt%) with a size range from 20 to 45 μm was used in this study. Coatings were prepared by high velocity oxy-fuel (HVOF) thermal spraying using a commercial MetJet III liquid fuel gun. Kerosene and nitrogen were used as the fuel and carrier gas respectively. To manufacture free-standing CoNiCrAlY coatings, the powder was sprayed onto to 800-grit pre-ground mild steel substrates with a dimension of 60 × 25 × 1.8 mm^3. The coatings were then debonded from the mild steel substrates to obtain free-standing coatings. For CoNiCrAlY coated IN738 samples, the IN738 substrates were machined to the same dimension as the mild steel substrates and were grit blasted with Al_2O_3 particles at a blasting pressure of 0.5 MPa to produce a rough surface for coating adherence. The composition of the as-received IN738 substrate is summarised in Table 1. The spraying parameters used for preparing CoNiCrAlY free-standing coatings and coatings on IN738 substrates are essentially identical except a reduced number of passes was employed to deposit CoNiCrAlY coatings onto IN738 substrates. The details of the HVOF spray parameters are tabulated in Table 2. The as-sprayed surface of the deposited coatings was ground by 800-grit sand papers to ensure a consistent surface roughness of approximate 1 μm. An initial heat treatment was given to the as-sprayed coatings prior to the isothermal oxidation. Samples were heat treated in a low pressure vacuum of 6.0×10^{-3} mbar for 2 h at 1100 °C. This heat treatment has been found to be effective in minimising the coating porosity and allowing the β phase to precipitate. Heat treated samples were then exposed to laboratory air at 1100 °C for times up to 100 h followed by natural air cooling.

2.2. Material characterisation

A FEI XL30 field emission gun scanning electron microscope (FEG-SEM) operated at an accelerating voltage of 20 kV was used for microstructural analysis. Free-standing

CoNiCrAlY coatings and coated IN738 samples before and after isothermal oxidation were mounted in a conductive resin, ground and polished to 1 μm surface finish, and imaged by backscattered electrons (BSE) and secondary electrons (SE). Semi-quantitative energy dispersive X-ray analysis (EDX) was utilised to analyse the elemental compositions of various phases. Image analysis was conducted to measure the phase fractions using ImageJ [63]. X-ray diffraction (XRD) was performed on a Bruker D-500 X-ray diffractometer at 40 kV and 25 mA using a Cu-*Kα* source with a wavelength of 0.15406 nm. The XRD scans were conducted in a 2θ range of 20°-100° with a step size of 0.02° and a counting time 4s per step.

2.3. Thermodynamic calculations

The phase equilibriums of CoNiCrAlY and IN738 were evaluated by Thermo-Calc. The compositions of CoNiCrAlY and IN378 were used as the inputs to obtain the phase equilibrium information in TCNI8 thermodynamic database. The temperature, pressure and system size are specified as 1100 °C, 1×10^5 Pa and 1 mole respectively as the equilibrium calculation conditions. Thermo-Calc employs a series of Gibbs free energy minimisation routines to calculate the equilibrium information at various states. The equilibrium information such as phase fraction against temperature or composition can be obtained. The phases considered in CoNiCrAlY were liquid, γ, γ', β-NiAl, σ whilst the phases covered in IN738 were liquid, γ, γ' and carbides. To evaluate the formation mechanisms of Al_2O_3, AlN and TiN in air at 1100 °C, the equilibrium phases with additions of Ti, N and O were calculated to demonstrate the thermodynamic reaction of bioxidant corrosion. The details of how Thermo-Calc works are given elsewhere [64].

3. Results

3.1. Microstructure characterisation

The microstructure of initial heat treated free-standing CoNiCrAlY coating is shown in Fig. 1. The coating, of approximately 400 μm in thickness as seen from Fig. 1a, exhibits a clear two-phase structure, consisting of the fcc γ-Ni matrix and the bcc β-NiAl secondary phase. The area fraction of the β-NiAl phase is measured to be around 30% by image analysis from Fig. 1b. Very little porosity is present in the coating, which agrees well with previously reported studies that the initial heat treatment can act as a sintering effect to reduce the coating porosity [46, 65]. Some dark contrast, micro sized particles are seen in the coating, with an area fraction less than 1%. They are either discrete particles or thin stringers and mostly distributed around the powder particle boundaries. Such features are presumably resulted from the oxidation of in-flight powder particles during the HVOF process and they are found to be aluminium oxides by chemical analysis. A small β-phase depletion zone is formed at the coating surface, which is likely resulted from pre-oxidation during the initial heat treatment. The microstructure of the CoNiCrAlY coated IN738 after initial heat treatment is depicted in Fig. 2. The coatings were sprayed with 16 passes and are found to be ~270 μm thick, as measured from Fig. 2a. It can be seen from Fig. 2b that a small β depletion zone has also formed after initial heat treatment and no other phases can be found near the surface. In the centre of the coating in Fig. 2c, the β-phase area fraction is found to be ~30%, which is similar to the free-standing coating. The oxide particles/stringers are still visible in the coating. At the coating/substrate interface in Fig. 2d, the interdiffusion zone (IDZ) has formed during heat treatment due to the β phase depletes to the IN738 substrate and the internal loss of the β phase occurs. Ti-rich precipitates which are confirmed by EDX analysis can be found near the IDZ. Fig. 3a presents the XRD patterns of initial heat treated free-standing CoNiCrAlY coating and CoNiCrAlY coated IN738. The two-phase γ+β structure is confirmed by Fig. 3a. Small amount of oxides peaks are identified in Fig. 3a, as indeed seen from Fig. 3b that a thin layer of oxides, presumably alumina, was formed after the heat treatment. This is possibly due to the relatively low vacuum quality (nominally 6.5×10^{-3} mbar) and pre-oxidation has

occurred during the heat treatment. The EDX analysis of the γ and β phase compositions is summarised in Table 3. The phase compositions in the CoNiCrAlY coating on IN738 are similar to the values that obtained from free-standing CoNiCrAlY coating. Y can be hardly detected due to its low content in the coating. A small amount of Ti is detected in the coating on IN738, which can be attributed to the diffusion of Ti from IN738 (3.4 wt%) to the CoNiCrAlY coating.

It has been reported that an initial heat treatment can facilitate the alumina scale growth during oxidation [38]. The initial alumina scale that formed during heat treatment acts as a stable diffusion barrier and reduces the oxygen activity at the coating surface. This is likely to prohibit the formation of spinel oxides and allow the alumina scale to grow in the subsequent oxidation. Similar heat treatment procedures have been employed in other studies and they have been demonstrated to have positive effects on the oxidation behaviour of CoNiCrAlY coatings [38, 39]. Thus, the above initial heat treated microstructures of free-standing CoNiCrAlY coating and coated IN738 are used as references to compare with the microstructure after high temperature exposures, in an attempt to reveal the substrate effects on the bioxidant corrosion behaviour of CoNiCrAlY coated IN738.

3.2. Isothermal oxidation of free-standing coating and coated IN738

Fig. 4 shows the microstructure evolution of heat treated CoNiCrAlY free-standing coatings after exposure in air at 1100 °C for various times. It is evident that a single oxide layer, predominantly alumina, is formed at the external coating surface. As discussed previously, the initial heat treatment can promote the formation of protective alumina. This is indeed seen in Fig. 4 as the oxide layer is only a single phase structure and it is found to be consisted of Al and O by chemical analysis. A β-phase depletion zone which only composes of γ phase is developed in contact with the oxide layer due to the loss of Al from the CoNiCrAlY coating to the alumina scale. The γ+β structure is visible when moving from the β-phase depletion

zone further down to the coating. No evidence of internal oxidation can be found in these free-standing coatings. This means the coatings still exhibit a good microstructural integrity after high temperature exposures. The XRD patterns of the oxidised CoNiCrAlY free-standing coatings are shown in Fig. 5. The majority of the oxides are identified as alumina, which agrees well with Fig. 4 that the oxide layer mainly consists of alumina whilst the evidence of spinel oxides can hardly be found.

The microstructure evolution of coated IN738 after high temperature exposure at 1100 °C is depicted in Fig. 6. A distinct difference in the oxidation behaviour between coated IN738 and free-standing CoNiCrAlY coating is noticed. No continuous and protective oxide layers can be found at the coating surface and significant internal bioxidation corrosion has occurred. The internal oxidation at the coating sub-surface mainly results in the formation of aluminium oxides. This is confirmed by the EDX mapping of the coating after 25 h exposure at 1100 °C in Fig. 7. These internal oxides exhibit irregular shapes and are distributed within approximately 10-15 μm immediately beneath the coating surface. They are probably the oxide-precipitates forming along the grain boundaries and exhibit no evidence of needle-like morphology. Furthermore, faceted and needle-like features are identified in the region below the internal oxides and they are found be to Al-rich nitrides. Thus, two unique zones are developed in the bioxidant corrosion of the coated IN738, namely the Al_2O_3-rich internal oxidation zone close to the coating surface and the AlN-rich internal nitridation zone beneath the internal oxidation zone. It is further seen from Fig. 6 that the internal nitridation zone has grown significantly after 100 h exposure. Discrete TiN particles are found in the interdiffusion zone close to the coating/substrate interface after 100 h exposure. The original bright contrast Ti-rich precipitate in the IN738 substrate has been corroded to TiN. This means nitrogen has penetrated the CoNiCrAlY coating and caused large areas of nitridation in the coating and substrate. To qualitatively analyse the compositions of AlN and TiN, at least five micrographs were taken and five EDX measurements were performed in each micrograph.

The approximate compositions of AlN and TiN are summarised in Table 4. Due to the uncertainties of EDX in quantifying the elemental composition, only the major elements in AlN and TiN are given in Table 4. It can be seen the major elements in AlN and TiN are Al&N and Ti&N respectively, which shows a good agreement with the reported STEM analysis of the AlN and TiN in a NiCrAlY coated Ni-based superalloy system [61]. Table 4 shows that the atomic ratios of Al:N and Ti:N in AlN and TiN are close to 1. It is also known that the β-NiAl in the CoNiCrAlY coating is rich in Al. The formation of AlN results in rapid depletion of the β-NiAl phase. Since the protective effect of the CoNiCrAlY coating is represented by the residual amount of the β phase in the coating, a comparison of the β-phase depletion between the free-standing coating and coated IN738 is presented in Fig. 8. The β-phase depletion zone is measured from the coating surface to the edge of the β phases. It is seen that the β-phase depletion is rather slow in the free-standing CoNiCrAlY coating but rapid consumption of the β phase occurs in the coated IN738 due to bioxidant corrosion. Fig. 9 presents the XRD patterns of coated IN738 after high temperature exposure in air at 1100 °C for times up to 100 h. Aluminium oxides are clearly identified and small amounts of Cr_2O_3 and spinel oxides are also identified. An increase in the intensity of aluminium oxides is seen after 75 h oxidation. The low intensity of nitride, mainly AlN and TiN, is likely due to the fact that internal nitridation zone is more than 10 μm away from the coating surface and the X-ray penetration depth is rather shallow [66]. Since the TiN is mainly found in the interdiffusion zone close to coating/substrate interface, which is further away from the coating surface, the intensity of the nitride peaks is not as high as that of Al_2O_3. But it is seen from Fig. 6 that the internal nitridation has significantly occurred after 100 h exposure. The β phase peaks have also been largely suppressed after the bioxidant corrosion. This agrees well with Fig. 8 that the β phase depletes rapidly in the coated IN738 due to the internal oxidation and nitridation.

3.3. Thermodynamic calculation of bioxidation corrosion

The bioxidation corrosion of the CoNiCrAlY+IN738 system consists of an internal oxidation and an internal nitridation processes. To demonstrate the formation of thermodynamically driven oxides and nitrides, thermodynamic calculations on the formation of Al_2O_3, AlN and TiN were performed using Thermo-Calc with TCNI8 database. The TCNI8 database is employed here since it is suitable for Ni-based alloys and includes the thermodynamic properties of AlN and TiN. Given the following chemical reactions are driven by the thermodynamic properties of Al_2O_3, AlN and TiN, the thermodynamic reactions below are evaluated by defining three individual systems that comprise Al&O, Al&N and Ti&N.

$$2Al + 3O = Al_2O_3 \quad (1)$$

$$Al + N = AlN \quad (2)$$

$$Ti + N = TiN \quad (3)$$

The size of each system is defined as 1 mole. In the formation of Al_2O_3, the mole percent of Al and O are 40% and 60%. In the formation of AlN, the mole percent of Al and N are 50% and 50%. Similarly, in the formation of TiN, the mole percent of Ti and N are also 50% and 50%. The pressure of the above reactions is kept at 1×10^5 Pa and the temperature range is 800-1200 °C. By using the Thermo-Calc with TCNI8 database, the thermodynamic values, enthalpy (ΔH^0) and Gibbs free energy (ΔG^0), in forming the Al_2O_3, AlN and TiN can be obtained, as summarised in Fig. 10. It can be seen that Al_2O_3 exhibits the largest ΔH^0 and ΔG^0, indicating that the formation of Al_2O_3 is likely to occur at the early stage. This is supported by the evidence that the internal oxidation zone which mainly consists of Al_2O_3 is close to the coating surface. Since ΔH^0 and ΔG^0 of AlN and TiN are smaller than that of Al_2O_3, the formation of nitrides may occur at a later stage, depending on the diffusion of N from the atmosphere and Ti from the IN738 substrate. Furthermore, the solubility of oxygen and nitrogen in this CoNiCrAlY coating may also influence the formation kinetics of internal Al_2O_3 and nitrides. The solubility limits of oxygen and nitrogen are commonly defined as the maximum amount of oxygen and nitrogen that can be taken up within the CoNiCrAlY coating

prior to the precipitation of any oxide or nitride, including Al_2O_3 and AlN. Due to the limited data available in the CoNiCrAlY coatings, such information on the solubility limits of oxygen and nitrogen can be referred to the work reported by Guan et al. as an approximation [67]. It is found that these values are quite small, generally less than 1%. The thicknesses of the internally reacted regions, x_i, can be approximated in Eq. (4) [57],

$$x_i = \sqrt{\frac{D_i C_i^s}{2\nu C_{Al}} t} \qquad (4)$$

where i represents the O and N, D_i is the diffusion coefficient, C_i^s is the solubility of oxygen and nitrogen, ν is the stoichiometric coefficient of the Al_2O_3 and AlN, taken as 1.5 and 1 respectively, C_{Al} is the initial concentration of the oxide and nitride forming element, taken as the Al concentration in the initial CoNiCrAlY composition, 8.1 wt%, t is the exposure time. Taking the values of $D_O C_O^S$ and $D_N C_N^S$ from Han et al. [59] and using the data stated above, the penetration depth of the internal oxidation zone and internal nitridation zone can be compared. This gives $x_O/x_N \sim 0.3$, indicating the internal nitridation zone is larger than the internal oxidation zone at the equilibrium state, which shows reasonable agreement with Fig. 6 after 100 h oxidation time. It should also be noted that the internally-formed Al_2O_3 can further reduce the solubility of oxygen in the CoNiCrAlY coating. As a result, the internal oxidation only occurs in the region close to the coating surface.

By knowing the thermodynamic properties of the internal oxides and nitrides, a further evaluation on the bioxidant corrosion can be conducted in the CoNiCrAlY+IN738 system. It is noticed from Fig. 6 that the bioxidant corrosion mainly occurs in the CoNiCrAlY coating. Since the interdiffusion has already occurred between the coating and substrate during the initial heat treatment and considering the grain size of this thermally sprayed CoNiCrAlY coating is reported to be 0.5~2 μm [26, 32], a Ti content which is assumed to be 3.4 wt% (all from the IN738 substrate) is included in the thermodynamic calculation of the CoNiCrAlY coating. Since N_2 and O_2 are free to contact with the coating, a CoNiCrAlTiNO multi-

component system is assumed here to investigate the phase equilibrium. The total system is assumed 1 mole and the mass ratio of N_2 to O_2 in the air is used here to represent the composition of N and O in the CoNiCrAlTiNO system. The mass ratio of N to O is kept to be 3.25, as this value is close to that in the air. Thus, the CoNiCrAlY with Ti, N and O is defined as Co-31.7Ni-20.8Cr-8.1Al-3.4Ti-3.25N-1O (all in wt%) as an approximation to calculate the phase equilibrium. The small amount of Y is neglected here. The volume fractions of the Al_2O_3 and nitrides can then be calculated, as summarised in Fig. 11. It can be seen the volume fractions of AlN and TiN are larger than Al_2O_3. Since the internal oxidation occurs at the early stage of bioxidant corrosion, the Al_2O_3 formed in the internal oxidation zone reduces the activity of oxygen from further chemical reaction. This allows nitrogen to be readily reacted with the rest of the coating. Subsequently, the nitrogen reacts with the Al-rich β phase in the CoNiCrAlY coating to form the AlN. Since the β phase exhibits a volume fraction of 30% in the coating, large areas of AlN is thus expected. This agrees well with Fig. 6 that the internal nitridation zone increases with oxidation time and serious nitridation occurs at long term exposures of 100 h. The inward diffusion of N and outward diffusion of Ti allow the thermodynamically stable TiN to form. This is also consistent with Fig. 6 that TiN has formed in the regions closed to the coating/substrate interface.

4. Discussion

The widely recognised oxidation behaviour of CoNiCrAlY coating is represented by its capability in forming a continuous and protective alumina scale at the coating surface, as indeed seen from Fig. 4. The bioxidant corrosion of CoNiCrAlY+IN738 occurs when no continuous and protective oxide can be formed at the surface. A solid molar volume change is expected during the formation of internal oxides. The internal oxidation reaction can be considered as a decomposition of the oxygen-saturated CoNiCrAlY coating. Using the

modelled composition from Fig. 11 and assuming all solution oxygen precipitates are alumina, the reaction can be given below (element in atomic fraction),

$Co_{0.251}Ni_{0.252}Cr_{0.186}Al_{0.140}Ti_{0.033}N_{0.108}O_{0.03}=0.01Al_2O_3+Co_{0.264}Ni_{0.265}Cr_{0.196}Al_{0.126}Ti_{0.035}N_{0.114}$ (5)

Taking 3.95 g/cm^3 and 7.46 g/cm^3 as the density of Al_2O_3 and CoNiCrAlY coating respectively [68] and utilizing the average molecular weights based on the above atomic fractions, the molar volume of each compound from left to right in the above reaction is approximately 6.25, 25.8 and 6.43 cm^3/mol. The net change in solid volume is then obtained as:

$$\frac{\Delta V}{V_0}=\frac{V_f-V_0}{V_0}\sim+7\% \quad (6)$$

This positive net increase in solid volume means that the volume expansion of the CoNiCrAlY coating is likely to occur during the internal oxidation process, indicating further internal reaction is possible. It is revealed from the thermodynamic calculations that the AlN is also a thermodynamically stable phase when N exists and the reaction of nitridation may start after oxidation from Fig. 10. Hence the internal nitridation zone can be formed underneath the internal oxidation zone in the Al-rich regions. As seen from Fig.6 that there are still a large amount of Al-rich β phase in the coating after early oxidation of 25 h but serious β-phase depletion occurs at long time exposures. This means the β phases are significantly consumed during the internal nitridation stages because the nitridation zone grows rapidly with exposure time. It has been reported that nitrogen becomes very active above 1100 °C [69], the Al in the β phase tend to react with nitrogen to form the thermodynamically stable AlN. Since the Al_2O_3 is more thermodynamically stable than AlN, a transition from AlN to Al_2O_3 is likely to occur after long term exposures. This is indeed supported by the evidence that the intensity of Al_2O_3 increases at 75 h in Fig. 9. Similar findings have also been reported by Liu et al. [61]. In the interdiffusion zone, where Ti is believed to be rich due to interdiffusion between the coating and substrate, nitrogen diffuses through the coating towards the substrate to react with Ti to form stable TiN. This produces

more driving force for further diffusion of nitrogen through the CoNiCrAlY+IN738 system. Eventually the Ti-rich precipitate in the IN738 is nitrided, as seen from Fig. 6, which can cause detrimental mechanical degradation of the system.

The bioxidant corrosion of MCrAlY coating systems has been reported in a few studies [61, 62]. Two common phenomena are noted when comparing to these studies, in which no continuous protective oxide can form at the surface and high Ti content exists in system. The free-standing CoNiCrAlY coatings act as the reference samples, showing no internal oxidation and nitridation occurs in the free-standing coatings. Such behaviour in MCrAlY coatings has been widely recognised and reported. Considering the exposure surface conditions are identical between the free-standing coatings and coated IN738, the dominant effects on the bioxidant corrosion of CoNiCrAlY are resulted from the IN738 substrate. Litz et al. [56] have reported the internal oxidation and nitridation behaviour of IN738 in air. They have found that the nitrogen is able to react with the Ti-rich carbides to form the TiN, which shows good consistency with Fig. 6 in this study. Similar findings were also reported in Ti-rich nickel-based alloys by Krupp et al. [57, 58]. It is thus believed that the Ti plays a predominant role in facilitating the bioxidant corrosion. From the thermodynamic calculations, it is shown that the AlN and TiN are also the thermodynamically stable phases. Since the samples were exposed in air at 1100 °C, nitrogen and oxygen can simultaneously contact the CoNiCrAlY coating. The thermodynamic driving force to form the nitrides is very high, resulting the nitrogen to diffuse through the CoNiCrAlY coating towards the IN738 substrate. The instant access of N_2 and O_2 in the coating causes the internal oxidation and nitridation, which indeed shortens the durability of CoNiCrAlY coating on high Ti-content IN738 substrates due to the rapid consumption of the β phase during the bioxidant corrosion process. However, this may not be the case for the free-standing CoNiCrAlY coating because no Ti exists in the free-standing coatings and the flux of N_2 towards the free-standing coating is not

as high as that in the CoNiCrAlY+IN738 system. Therefore, the evidence of internal oxidation and nitridation is not found in the free-standing coatings.

5. Conclusions

The bioxidant corrosion behaviour of CoNiCrAlY coated IN738 were investigated during isothermal oxidation at 1100 °C. The oxidation behaviour of CoNiCrAlY coated IN738 was compared with free-standing CoNiCrAlY coatings. The main conclusions were drawn below:

- It is found that bioxidant corrosion occurs in the CoNiCrAlY coated IN738, in which an internal oxidation zone and an internal nitridation zone are developed in the CoNiCrAlY coating. No evidence of bioxidant corrosion can be found in the free-standing CoNiCrAlY coating.
- The internal nitridation zone mainly forms underneath the internal oxidation zone and it grows with oxidation time, causing significant depletion of β phase in the CoNiCrAlY coating. This is likely driven by the thermodynamic force to form more stable AlN and TiN in the system.
- Ti-rich TiN is found near the coating and substrate interface after long term exposures and nitridation of Ti-rich precipitates in the substrate has also occurred. This is due to further diffusion of nitrogen through the coating towards the substrate, allowing more nitridation to occur.
- It is believed that the internal oxidation and nitridation occurs when no protective oxides can be formed at the CoNiCrAlY coating surface. The volume expansion of the internal oxidation and nitridation causes the bioxidant corrosion behaviour to the CoNiCrAlY coating on IN738, which results in significant reduction in the lifetime of the CoNiCrAlY coating.

Declaration of interest

Declarations of interest: none

Data availability

The raw/processed data required to reproduce these findings cannot be shared at this time as the data also forms part of an ongoing study.

Acknowledgements

The authors would like to thank Prof. John Nicholls, Prof. Graham McCartney and Dr. Katy Voisey for valuable discussions. The authors would like to acknowledge Prof. Graham McCartney for providing the access to the Thermo-Calc computing facilities at the Faculty of Engineering, University of Nottingham. This research was supported by Zhejiang Provincial Natural Science Foundation of China under Grant No. LQ18E010002, Ningbo Natural Science Foundation under Grant No. 2018A610168 and Qianjiang Talent Scheme under Grant No. QJD1803012.

References

[1] J.R. Nicholls, N.J. Simms, W.Y. Chan, H.E. Evans, Smart overlay coatings — concept and practice, Surf. Coat. Technol. 149 (2002) 236-244.
[2] J.R. Nicholls, Designing oxidation-resistant coatings, JOM 52 (2000) 28-35.
[3] Y. Chen, X. Zhao, M. Bai, L. Yang, C. Li, L. Wang, J.A. Carr, P. Xiao, A mechanistic understanding on rumpling of a NiCoCrAlY bond coat for thermal barrier coating applications, Acta Mater. 128 (2017) 31-42.
[4] M.J. Pomeroy, Coatings for gas turbine materials and long term stability issues, Mater. Des. 26 (2005) 223-231.
[5] E.A.G. Shillington, D.R. Clarke, Spalling failure of a thermal barrier coating associated with aluminum depletion in the bond-coat, Acta Mater. 47 (1999) 1297-1305.
[6] H. Chen, T.H. Hyde, K.T. Voisey, D.G. McCartney, Application of small punch creep testing to a thermally sprayed CoNiCrAlY bond coat, Mater. Sci. Eng. A 585 (2013) 205-213.
[7] M. Ansari, R. Shoja-Razavi, M. Barekat, H.C. Man, High-temperature oxidation behavior of laser-aided additively manufactured NiCrAlY coating, Corros. Sci. 118 (2017) 168-177.
[8] L. Luo, X. Shan, Z. Zou, C. Zhao, X. Wang, A. Zhang, X. Zhao, F. Guo, P. Xiao, A high performance NiCoCrAlY bond coat manufactured using laser powder deposition, Corros. Sci. 126 (2017) 356-365.

[9] A.G. Evans, D.R. Mumm, J.W. Hutchinson, G.H. Meier, F.S. Pettit, Mechanisms controlling the durability of thermal barrier coatings, Prog. Mater. Sci. 46 (2001) 505-553.
[10] H. Chen, T.H. Hyde, Use of multi-step loading small punch test to investigate the ductile-to-brittle transition behaviour of a thermally sprayed CoNiCrAlY coating, Mater. Sci. Eng. A 680 (2017) 203-209.
[11] J. He, H. Peng, S. Gong, H. Guo, Synergistic effect of reactive element co-doping in two-phase (γ' + β) Ni-Al alloys, Corros. Sci. 120 (2017) 130-138.
[12] R. Darolia, Thermal barrier coatings technology: critical review, progress update, remaining challenges and prospects, Int. Mater. Rev. 58 (2013) 315-348.
[13] H. Chen, G.A. Jackson, W. Sun, An Overview of Using Small Punch Testing for Mechanical Characterization of MCrAlY Bond Coats, J. Therm. Spray Technol. 26 (2017) 1222-1238.
[14] J. Wang, M. Chen, Y. Cheng, L. Yang, Z. Bao, L. Liu, S. Zhu, F. Wang, Hot corrosion of arc ion plating NiCrAlY and sputtered nanocrystalline coatings on a nickel-based single-crystal superalloy, Corros. Sci. 123 (2017) 27-39.
[15] J. Sun, S.M. Jiang, H.J. Yu, S.B. Liu, J. Gong, C. Sun, Oxidation behaviour of Pt modified aluminized NiCrAlYSi coating on a Ni-based single crystal superalloy, Corros. Sci. 139 (2018) 172-184.
[16] H. Chen, A. Rushworth, W. Sun, J. He, H. Guo, Some considerations in using the small punch testing for thermally sprayed CoNiCrAlY coatings, Surf. Coat. Technol. 357 (2019) 684-690.
[17] A. Hesnawi, H. Li, Z. Zhou, S. Gong, H. Xu, Isothermal oxidation behaviour of EB-PVD MCrAlY bond coat, Vacuum 81 (2007) 947-952.
[18] R.G. Wellman, A. Scrivani, G. Rizzi, A. Weisenburger, F.H. Tenailleau, J.R. Nicholls, Pulsed electron beam treatment of MCrAlY bondcoats for EB PVD TBC systems part 2 of 2: Cyclic oxidation of the coatings, Surf. Coat. Technol. 202 (2007) 709-713.
[19] P. Richer, M. Yandouzi, L. Beauvais, B. Jodoin, Oxidation behaviour of CoNiCrAlY bond coats produced by plasma, HVOF and cold gas dynamic spraying, Surf. Coat. Technol. 204 (2010) 3962-3974.
[20] H. Chen, G.A. Jackson, K.T. Voisey, D.G. McCartney, Modelling and experimental study on β-phase depletion behaviour of HVOF sprayed free-standing CoNiCrAlY coatings during oxidation, Surf. Coat. Technol. 291 (2016) 34-42.
[21] E. Hejrani, D. Sebold, W.J. Nowak, G. Mauer, D. Naumenko, R. Vaßen, W.J. Quadakkers, Isothermal and cyclic oxidation behavior of free standing MCrAlY coatings manufactured by high-velocity atmospheric plasma spraying, Surf. Coat. Technol. 313 (2017) 191-201.
[22] H. Chen, D.G. McCartney, Some aspects on modelling of the β-phase depletion behaviour under different oxide growth kinetics in HVOF CoNiCrAlY coatings, Surf. Coat. Technol. 313 (2017) 107-114.
[23] A. Gil, D. Naumenko, R. Vassen, J. Toscano, M. Subanovic, L. Singheiser, W.J. Quadakkers, Y-rich oxide distribution in plasma sprayed MCrAlY-coatings studied by SEM with a cathodoluminescence detector and Raman spectroscopy, Surf. Coat. Technol. 204 (2009) 531-538.
[24] D. Naumenko, R. Pillai, A. Chyrkin, W.J. Quadakkers, Overview on Recent Developments of Bondcoats for Plasma-Sprayed Thermal Barrier Coatings, J. Therm. Spray Technol. 26 (2017) 1743-1757.
[25] T.J. Nijdam, W.G. Sloof, Modelling of composition and phase changes in multiphase alloys due to growth of an oxide layer, Acta Mater. 56 (2008) 4972-4983.
[26] H. Chen, T. Barman, Thermo-Calc and DICTRA modelling of the β-phase depletion behaviour in CoNiCrAlY coating alloys at different Al contents, Comput. Mater. Sci. 147 (2018) 103-114.

[27] E.Y. Lee, D.M. Chartier, R.R. Biederman, R.D. Sisson, Modelling the microstructural evolution and degradation of M-Cr-Al-Y coatings during high temperature oxidation, Surf. Coat. Technol. 32 (1987) 19-39.
[28] K. Yuan, R. Eriksson, R. Lin Peng, X.-H. Li, S. Johansson, Y.-D. Wang, MCrAlY coating design based on oxidation-diffusion modelling. Part I: Microstructural evolution, Surf. Coat. Technol. 254 (2014) 79-96.
[29] R. Eriksson, K. Yuan, X.-H. Li, R. Lin Peng, MCrAlY coating design based on oxidation–diffusion modelling. Part II: Lifing aspects, Surf. Coat. Technol. 253 (2014) 27-37.
[30] M.S.A. Karunaratne, S. Kyaw, A. Jones, R. Morrell, R.C. Thomson, Modelling the coefficient of thermal expansion in Ni-based superalloys and bond coatings, J. Mater. Sci. 51 (2016) 4213-4226.
[31] M.S.A. Karunaratne, I. Di Martino, S.L. Ogden, D.L. Oates, R.C. Thomson, Modeling of Microstructural Evolution in an MCrAlY Overlay Coating on Different Superalloy Substrates, Metall. Mater. Trans. A 43 (2011) 774-788.
[32] H. Chen, Application of Precipitate Free Zone Growth Kinetics to the β-Phase Depletion Behavior in a CoNiCrAlY Coating Alloy: An Analytical Approach, Metall. Mater. Trans. A 49 (2018) 2551-2560.
[33] M.S.A. Karunaratne, S.L. Ogden, S.D. Kenny, R.C. Thomson, A multicomponent diffusion model for prediction of microstructural evolution in coated Ni based superalloy systems, Mater. Sci. Technol. 25 (2009) 287-299.
[34] M. Subanovic, D. Sebold, R. Vassen, E. Wessel, D. Naumenko, L. Singheiser, W.J. Quadakkers, Effect of manufacturing related parameters on oxidation properties of MCrAlY-bondcoats, Mater. Corros. 59 (2008) 463-470.
[35] B. Rajasekaran, G. Mauer, R. Vaßen, Enhanced Characteristics of HVOF-sprayed MCrAlY Bond Coats for TBC Applications, J. Therm. Spray Technol. 20 (2011) 1209-1216.
[36] M. Tahari, M. shamanian, M. salehi, The effect of heat treatment and thermal spray processes on the grain growth of nanostructured composite CoNiCrAlY/YSZ powders, J. Alloys Compd. 646 (2015) 372-379.
[37] A. Gil, V. Shemet, R. Vassen, M. Subanovic, J. Toscano, D. Naumenko, L. Singheiser, W.J. Quadakkers, Effect of surface condition on the oxidation behaviour of MCrAlY coatings, Surf. Coat. Technol. 201 (2006) 3824-3828.
[38] D. Salehi Doolabi, M.R. Rahimipour, M. Alizadeh, S. Pouladi, S.M.M. Hadavi, M.R. Vaezi, Effect of high vacuum heat treatment on microstructure and cyclic oxidation resistance of HVOF-CoNiCrAlY coatings, Vacuum 135 (2017) 22-33.
[39] S. Saeidi, K.T. Voisey, D.G. McCartney, The Effect of Heat Treatment on the Oxidation Behavior of HVOF and VPS CoNiCrAlY Coatings, J. Therm. Spray Technol. 18 (2009) 209-216.
[40] C.S. Richard, G. Béranger, J. Lu, J.F. Flavenot, The influences of heat treatments and interdiffusion on the adhesion of plasma-sprayed NiCrAlY coatings, Surf. Coat. Technol. 82 (1996) 99-109.
[41] P. Puetz, X. Huang, R.S. Lima, Q. Yang, L. Zhao, Characterization of transient oxide formation on CoNiCrAlY after heat treatment in vacuum and air, Surf. Coat. Technol. 205 (2010) 647-657.
[42] T. Mori, S. Kuroda, H. Murakami, H. Katanoda, Y. Sakamoto, S. Newman, Effects of initial oxidation on β phase depletion and oxidation of CoNiCrAlY bond coatings fabricated by warm spray and HVOF processes, Surf. Coat. Technol. 221 (2013) 59-69.
[43] G. Mauer, D. Sebold, R. Vaßen, E. Hejrani, D. Naumenko, W.J. Quadakkers, Impact of processing conditions and feedstock characteristics on thermally sprayed MCrAlY bondcoat properties, Surf. Coat. Technol. 318 (2017) 114-121.
[44] J. Toscano, R. Vaen, A. Gil, M. Subanovic, D. Naumenko, L. Singheiser, W.J. Quadakkers, Parameters affecting TGO growth and adherence on MCrAlY-bond coats for TBC's, Surf. Coat. Technol. 201 (2006) 3906-3910.

[45] N. Czech, M. Juez-Lorenzo, V. Kolarik, W. Stamm, Influence of the surface roughness on the oxide scale formation on MCrAlY coatings studied in situ by high temperature X-ray diffraction, Surf. Coat. Technol. 108-109 (1998) 36-42.
[46] H. Chen, Microstructure characterisation of un-melted particles in a plasma sprayed CoNiCrAlY coating, Mater. Charact. 136 (2018) 444-451.
[47] R.D. Jackson, M.P. Taylor, H.E. Evans, X.-H. Li, Oxidation study of an EB-PVD MCrAlY thermal barrier coating system, Oxid. Met. 76 (2011) 259-271.
[48] B. Wang, J. Gong, A.Y. Wang, C. Sun, R.F. Huang, L.S. Wen, Oxidation behaviour of NiCrAlY coatings on Ni-based superalloy, Surf. Coat. Technol. 149 (2002) 70-75.
[49] J. Toscano, D. Naumenko, A. Gil, L. Singheiser, W.J. Quadakkers, Parameters affecting TGO growth rate and the lifetime of TBC systems with MCrAlY-bondcoats, Mater. Corros. 59 (2008) 501-507.
[50] K. Yuan, Y. Yu, J.-F. Wen, A study on the thermal cyclic behavior of thermal barrier coatings with different MCrAlY roughness, Vacuum 137 (2017) 72-80.
[51] G. Marginean, D. Utu, Cyclic oxidation behaviour of different treated CoNiCrAlY coatings, Appl. Surf. Sci. 258 (2012) 8307-8311.
[52] B.-Y. Zhang, G.-H. Meng, G.-J. Yang, C.-X. Li, C.-J. Li, Dependence of scale thickness on the breaking behavior of the initial oxide on plasma spray bond coat surface during vacuum pre-treatment, Appl. Surf. Sci. 397 (2017) 125-132.
[53] D. Seo, K. Ogawa, Y. Suzuki, K. Ichimura, T. Shoji, S. Murata, Comparative study on oxidation behavior of selected MCrAlY coatings by elemental concentration profile analysis, Appl. Surf. Sci. 255 (2008) 2581-2590.
[54] P. Niranatlumpong, C.B. Ponton, H.E. Evans, The Failure of Protective Oxides on Plasma-Sprayed NiCrAlY Overlay Coatings, Oxid. Met. 53 (2000) 241-258.
[55] A.K. Ray, D.K. Das, B. Venkataraman, P.K. Roy, B. Goswami, N. Roy, S.K. Das, N. Parida, S. Tarafder, S. Chaudhuri, S.K. Sahay, R.N. Ghosh, Characterization of rupture and fatigue resistance of TBC superalloy for combustion liners, Mater. Sci. Eng. A 405 (2005) 194-200.
[56] J. Litz, A. Rahmel, M. Schorr, Selective carbide oxidation and internal nitridation of the Ni-base superalloys IN 738 LC and IN 939 in air, Oxid. Met. 30 (1988) 95-105.
[57] U. Krupp, H.J. Christ, Internal Nitridation of Nickel-Base Alloys. Part I. Behavior of Binary and Ternary Alloys of the Ni-Cr-Al-Ti System, Oxid. Met. 52 (1999) 277-298.
[58] U. Krupp, H.J. Christ, Internal Nitridation of Nickel-Base Alloys. Part II. Behavior of Quaternary Ni-Cr-Al-Ti Alloys and Computer-Based Description, Oxid. Met. 52 (1999) 299-320.
[59] S. Han, D.J. Young, Simultaneous Internal Oxidation and Nitridation of Ni–Cr–Al Alloys, Oxid. Met. 55 (2001) 223-242.
[60] Bennett M. J., Newton R., Nicholls J. R., The behaviour of commercial FeCrAlRE alloys in nitrogen-oxygen – water vapour bioxidant environments, Mater. High Temp. 20 (2003) 347-356.
[61] Y.Z. Liu, X.B. Hu, S.J. Zheng, Y.L. Zhu, H. Wei, X.L. Ma, Microstructural evolution of the interface between NiCrAlY coating and superalloy during isothermal oxidation, Mater. Des. 80 (2015) 63-69.
[62] L. Shi, L. Xin, X. Wang, X. Wang, H. Wei, S. Zhu, F. Wang, Influences of MCrAlY coatings on oxidation resistance of single crystal superalloy DD98M and their inter-diffusion behaviors, J. Alloys Compd. 649 (2015) 515-530.
[63] C.A. Schneider, W.S. Rasband, K.W. Eliceiri, NIH Image to ImageJ: 25 years of image analysis, Nat. Methods 9 (2012) 671-675.
[64] J.O. Andersson, T. Helander, L. Höglund, P. Shi, B. Sundman, Thermo-Calc & DICTRA, computational tools for materials science, Calphad 26 (2002) 273-312.
[65] S. Saeidi, K.T. Voisey, D.G. McCartney, Mechanical Properties and Microstructure of VPS and HVOF CoNiCrAlY Coatings, J. Therm. Spray Technol. 20 (2011) 1231–1243.

[66] Y. Waseda, E. Matsubara, K. Shinoda, X-Ray Diffraction Crystallography, Springer, Berlin Heidelberg, 2011.
[67] S.W. Guan, W.W. Smeltzer, Oxygen solubility and a criterion for the transition from internal to external oxidation of ternary alloys, Oxid. Met. 42 (1994) 375-391.
[68] H. Chen, Y.Q. Si, D.G. McCartney, An analytical approach to the β-phase coarsening behaviour in a thermally sprayed CoNiCrAlY bond coat alloy, J. Alloys Compd. 704 (2017) 359-365.
[69] P. Kofstad, High-temperature oxidation of metals, Wiley, New York, 1966.

Table 1

The composition of as-received IN738 substrate.

Nominal composition, wt%												
Alloy	Ni	C	Cr	Co	Mo	Al	B	Ti	Ta	W	Zr	Nb
IN738	Bal.	0.17	16	8.5	1.75	3.4	0.01	3.4	1.75	2.6	0.1	0.9

Table 2

The HVOF spraying parameters of the free-standing CoNiCrAlY coating and CoNiCrAlY coated IN738.

HVOF spray parameters	Free-standing CoNiCrAlY coating	CoNiCrAlY coated IN738
Spray distance (mm)	356	356
Nozzle length (mm)	100	100
Kerosene flow rate (ml/min)	470	470
N_2 gas flow rate (l/min)	4.3	4.3
O_2 gas flow rate (l/min)	890	890
Powder feed rate (g/min)	64	64
Number of passes	30	16
Stoichiometry	98%	98%

Table 3

γ and β phase compositions of heat treated free-standing CoNiCrAlY coating and CoNiCrAlY coating on IN738.

Elements		γ phase		β phase	
		wt%	at%	wt%	at%
Free-standing CoNiCrAlY coating	Co	41.4	38.3	25.2	20.5
	Ni	29.0	26.9	48.2	39.3
	Cr	25.7	27.0	8.2	7.6
	Al	3.9	7.8	18.4	32.6
CoNiCrAlY coating on IN378	Co	40.4	37.4	23.9	19.3
	Ni	29.5	27.4	49.0	39.7
	Cr	25.4	26.6	8.0	7.4
	Al	3.7	7.5	19.1	33.6
	Ti	1.0	1.1	---	---

Table 4

The EDX measurements of the major elements in AlN and TiN.

Elements		Al	Ti	N
AlN	wt%	57.9±4.4	----	31.7±2.7
	at%	46.3±2.2	----	48.8±2.2
TiN	wt%	----	51.2±3.8	18.3±2.5
	at%	----	37.1±2.6	40.9±1.7

Figure captions

Fig. 1. The microstructure of initial heat treated free-standing CoNiCrAlY coating, (a) overall structure at low magnification and (b) a two-phase γ and β structure at high magnification.

Fig. 2. The microstructure of the CoNiCrAlY coated IN738 after initial heat treatment, (a) overall structure at low magnification, (b) the initial β-phase depletion zone at the coating surface, (c) the two-phase γ+β structure in the centre of the coating and (d) the interdiffusion zone at the coating/substrate interface.

Fig. 3. XRD patterns of initial heat treated free-standing CoNiCrAlY coating and CoNiCrAlY coated IN738 (a) and the microscopic image showing surface of coating after initial heat treatment (b)

Fig. 4. The microstructure of heat treated CoNiCrAlY free-standing coatings after oxidation exposure in air at 1100 °C for 25 h (a), 50 h (b), 75 h (c) and 100 h (d).

Fig. 5. XRD patterns of free-standing CoNiCrAlY coatings for different oxidation times at 1100 °C.

Fig. 6. The microstructure evolution of coated IN738 after high temperature exposure at 1100 °C, showing the bioxidant corrosion behaviour of internal oxidation and internal nitridation. Images from left to right represent the overall structure, coating surface, coating centre and coating/substrate interface.

Fig. 7. EDX mapping of internal oxidation zone and internal nitridation zone of coated IN738 after 25 h exposure in air at 1100 °C.

Fig. 8. Plot of the β-phase depletion in the free-standing CoNiCrAlY coating and CoNiCrAlY coated IN738 after oxidation in air at 1100 °C for times up to 100 h.

Fig. 9. XRD patterns of CoNiCrAlY coated IN738 after high temperature exposure in air at 1100 °C for times up to 100 h.

Fig. 10. Plots of enthalpy (a) and Gibbs free energy (b) of the thermodynamic reaction in forming the Al_2O_3, AlN and TiN. The ratios of mole percent in Al:O, Al:N and Ti:N are 2:3, 1:1 and 1:1 respectively in three individual systems which consist of Al&O, Al&N and Ti&N.

Fig. 11. Volume fraction of Al_2O_3, AlN and TiN in a composition of Co-31.7Ni-20.8Cr-8.1Al-3.4Ti-3.25N-1O (wt%) at different temperatures.

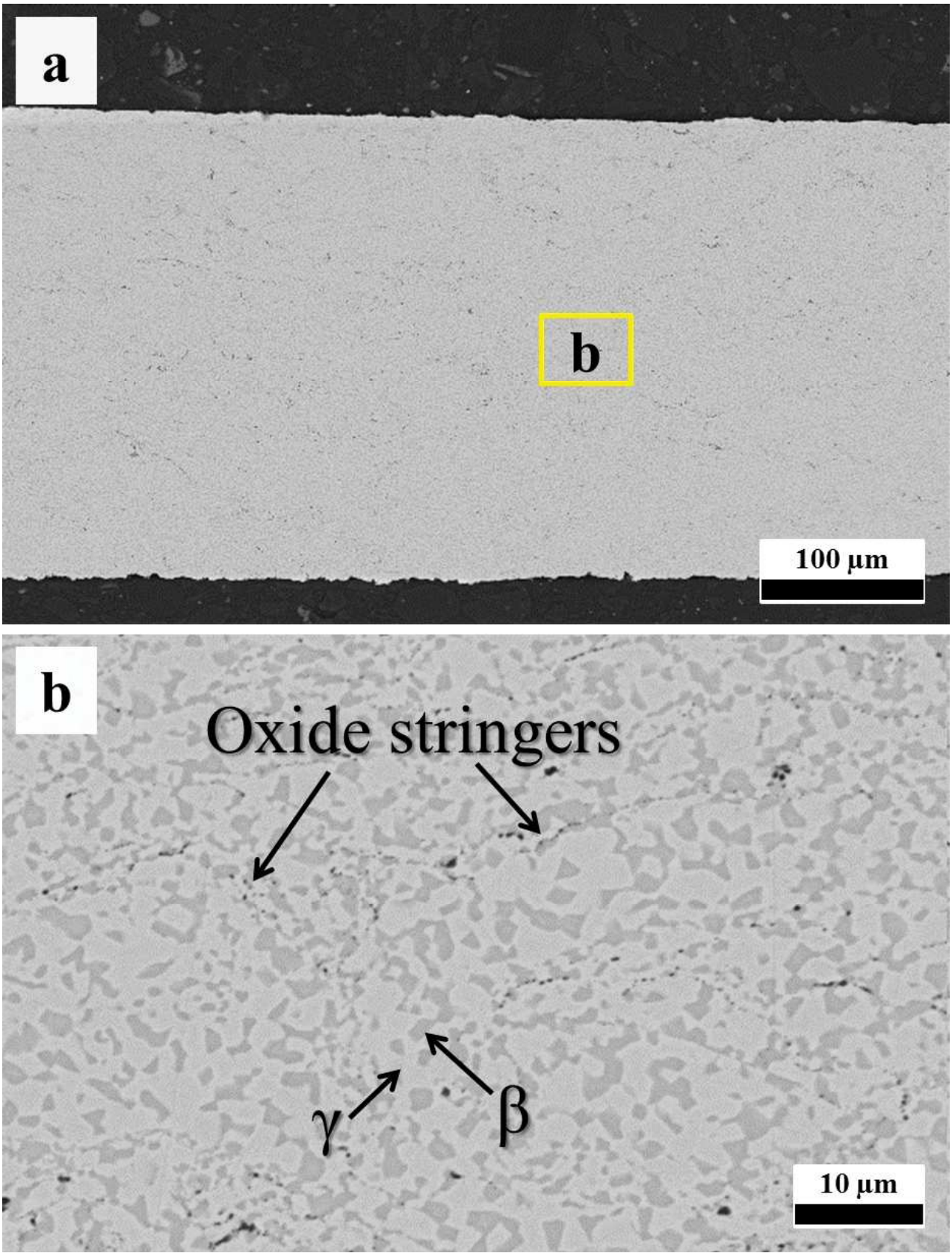
a
b
100 µm
b
Oxide stringers
γ
β
10 µm

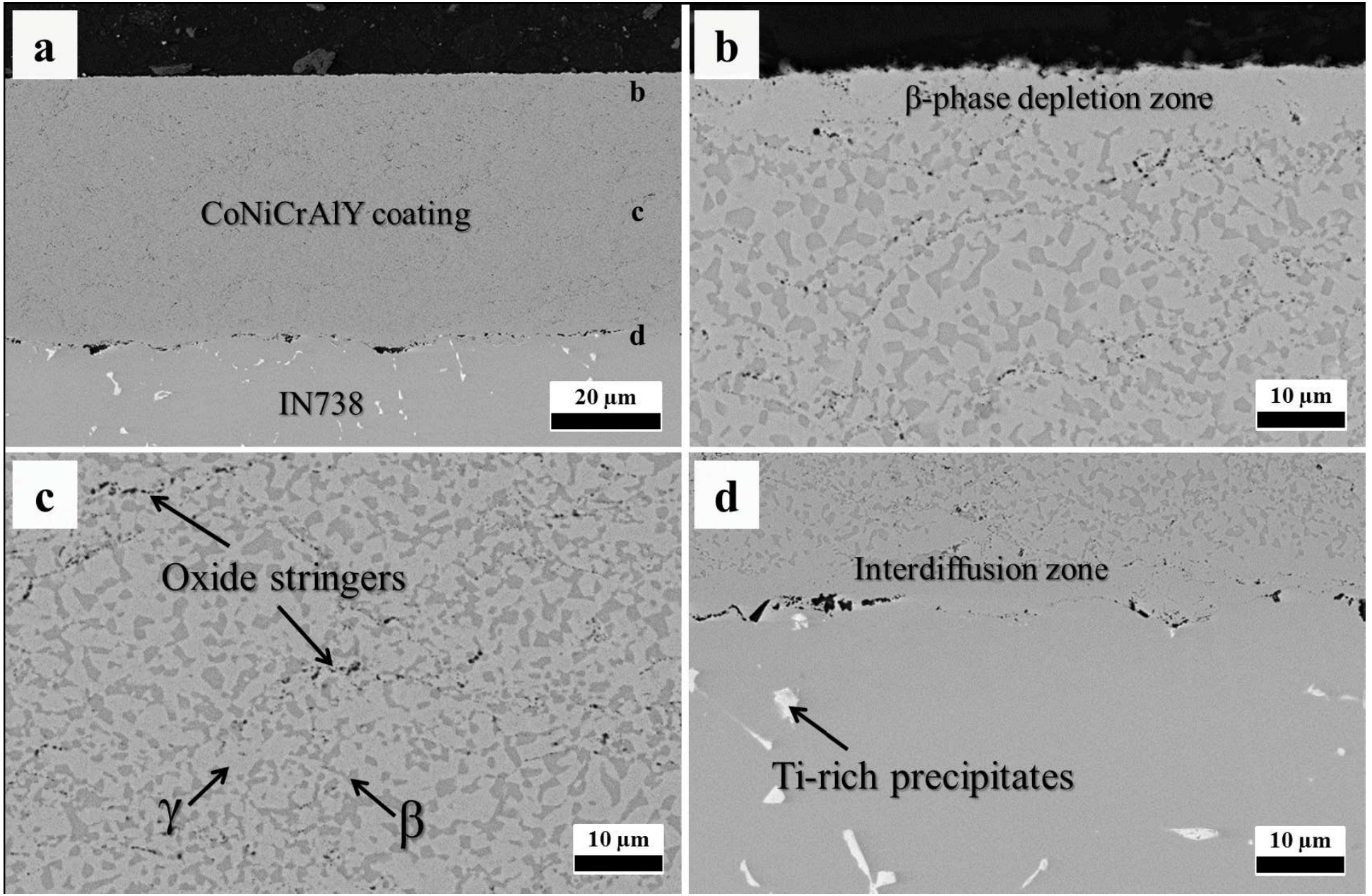
a
b
CoNiCrAlY coating
c
d
IN738
20 µm
b
β-phase depletion zone
10 µm
c
Oxide stringers
γ
β
10 µm
d
Interdiffusion zone
Ti-rich precipitates
10 µm

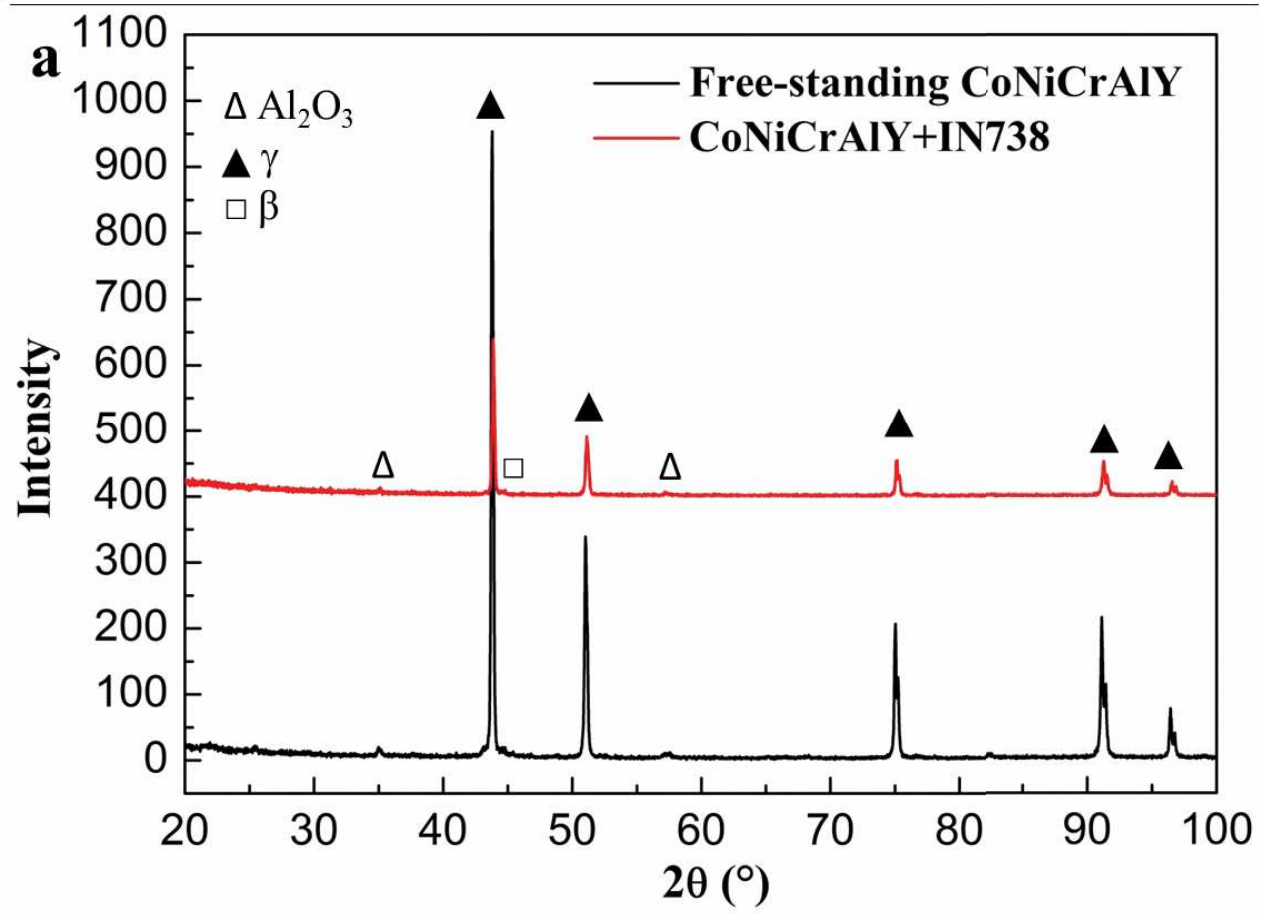
a
Δ Al2O3
▲ γ
□ β
Free-standing CoNiCrAlY
CoNiCrAlY+IN738
Intensity
2θ (°)
0
100
200
300
400
500
600
700
800
900
1000
1100
20
30
40
50
60
70
80
90
100

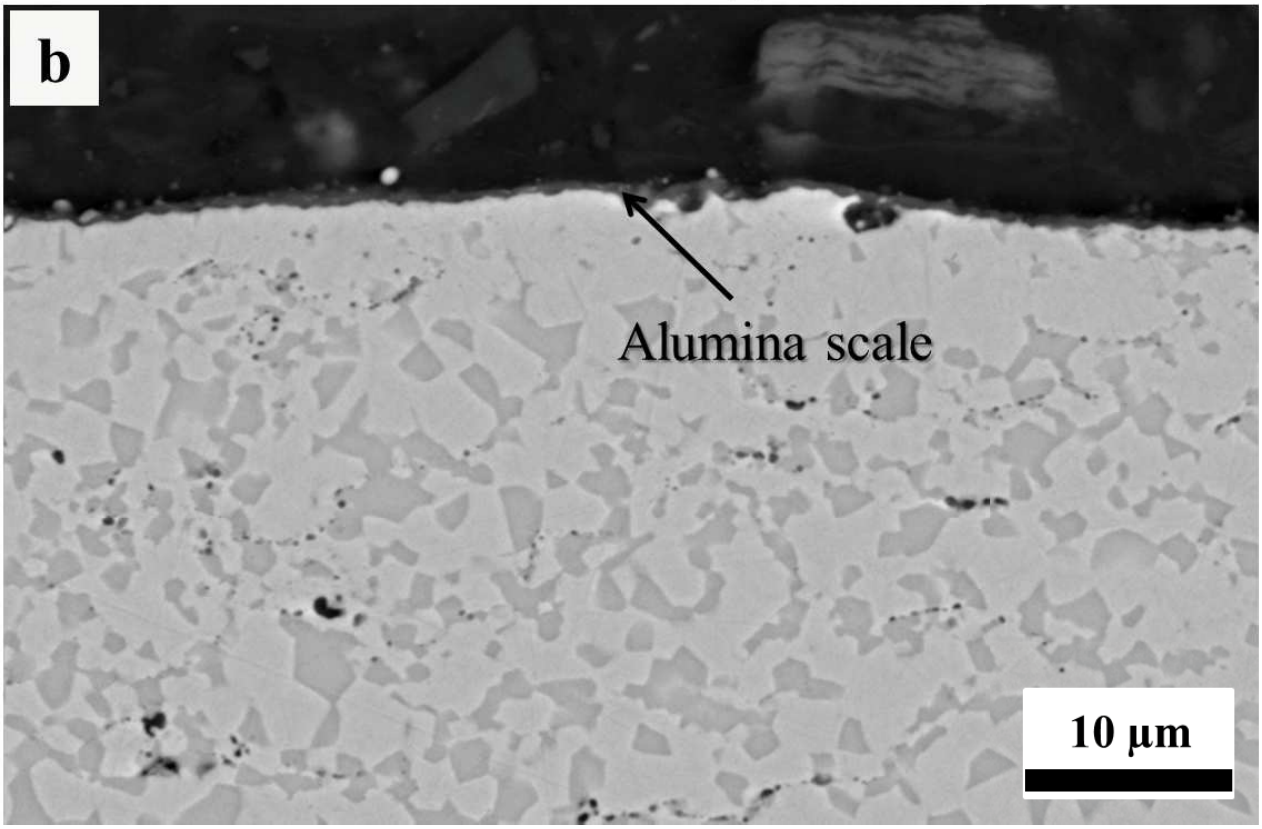
b
Alumina scale
10 μm

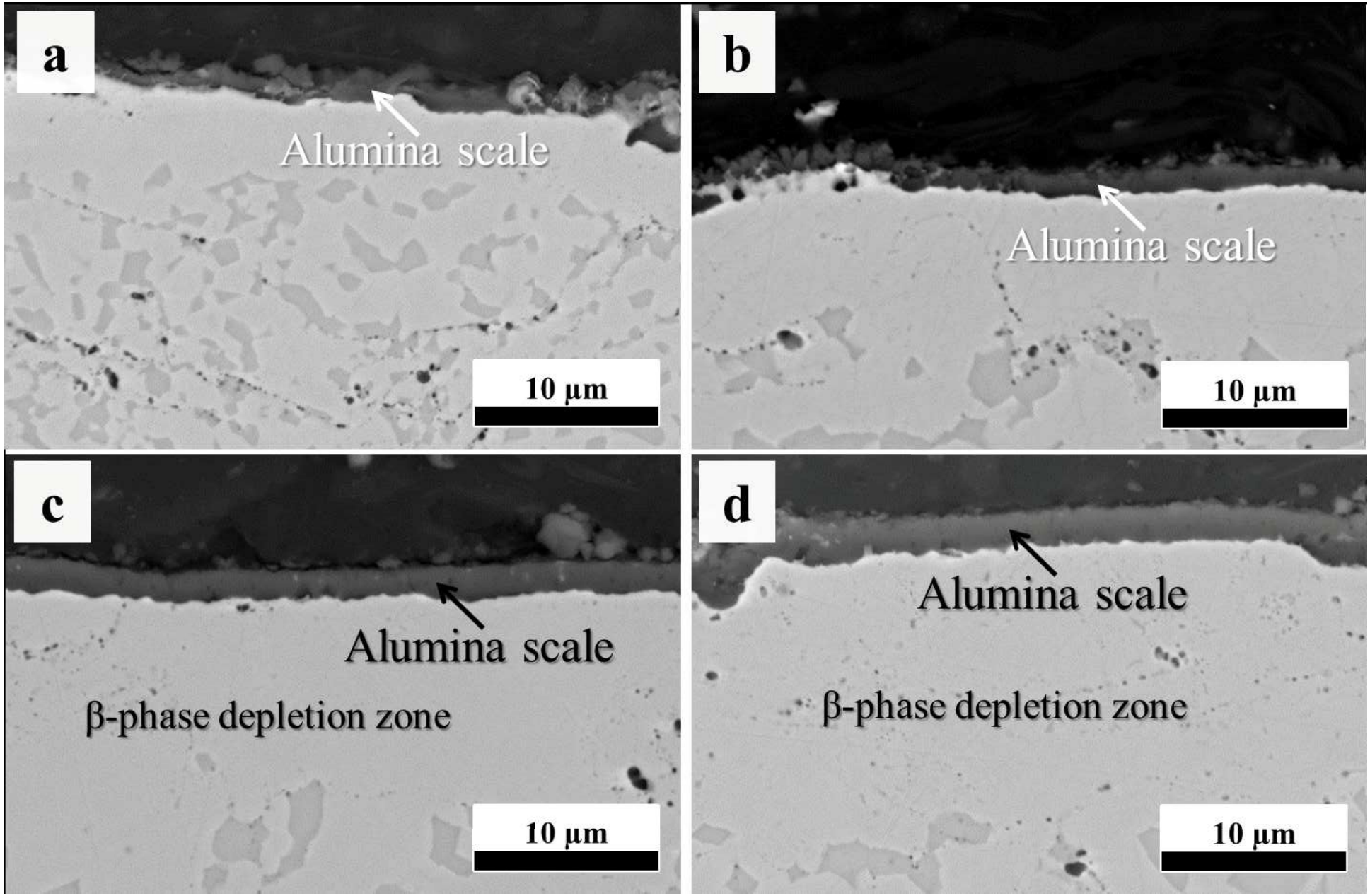
a
Alumina scale
10 µm
b
Alumina scale
10 µm
c
Alumina scale
β-phase depletion zone
10 µm
d
Alumina scale
β-phase depletion zone
10 µm

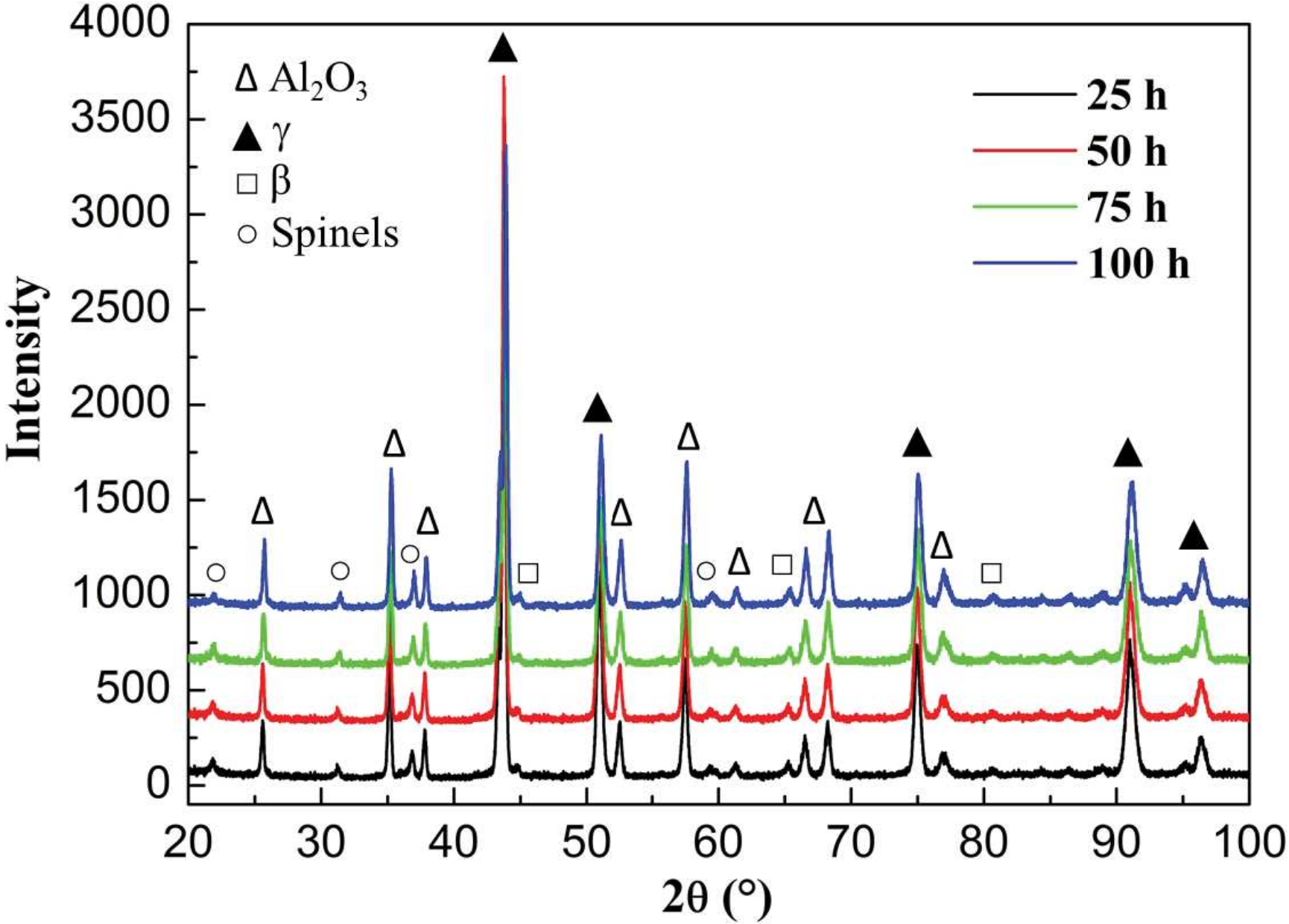
Δ Al2O3
▲ γ
□ β
○ Spinels
25 h
50 h
75 h
100 h
Intensity
2θ (°)
0
500
1000
1500
2000
2500
3000
3500
4000
20
30
40
50
60
70
80
90
100

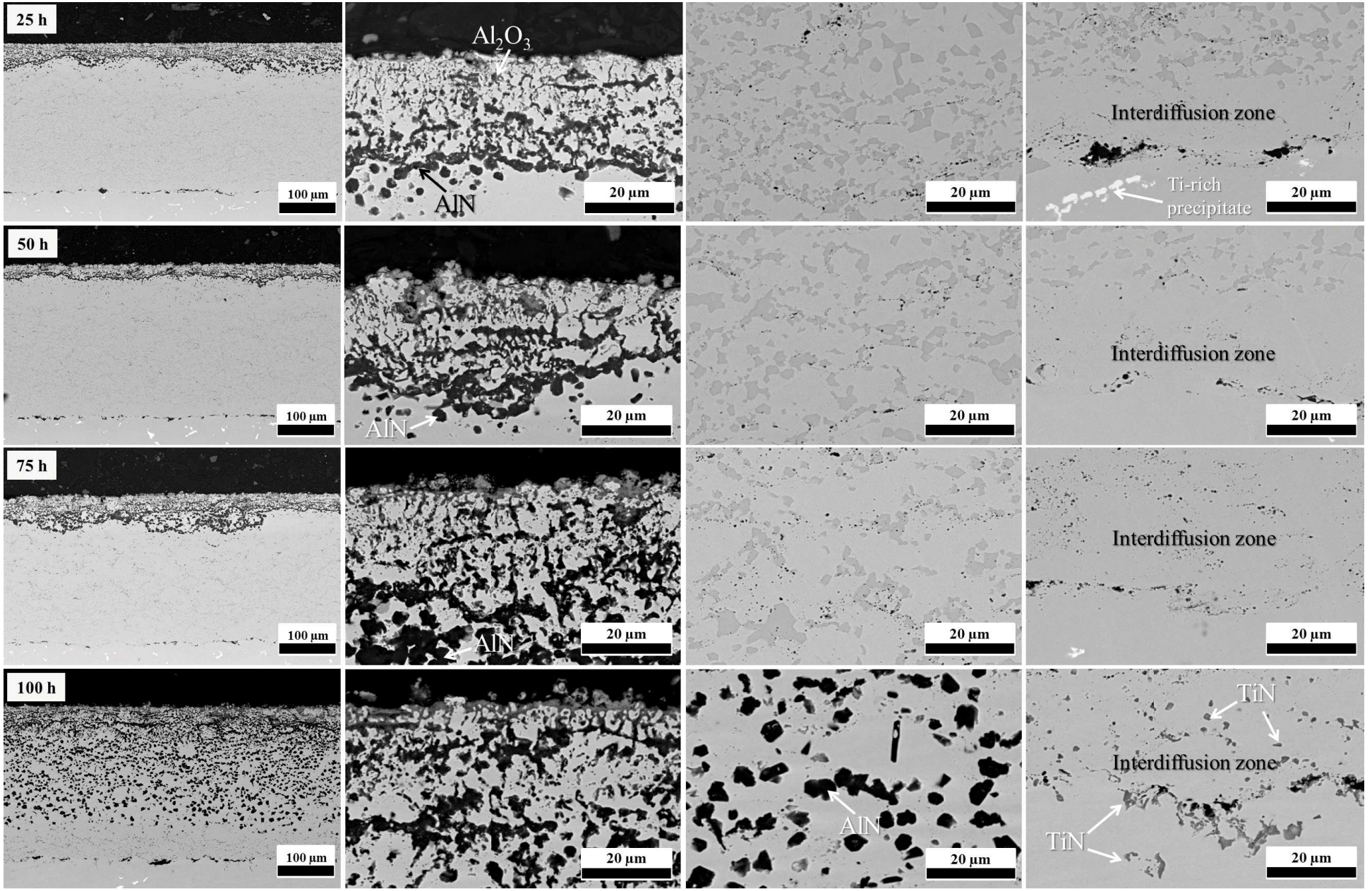
25 h
100 µm
Al_2O_3
AlN
20 µm
20 µm
Interdiffusion zone
Ti-rich
precipitate
20 µm
50 h
100 µm
AlN
20 µm
20 µm
Interdiffusion zone
20 µm
75 h
100 µm
AlN
20 µm
20 µm
Interdiffusion zone
20 µm
100 h
100 µm
20 µm
AlN
20 µm
TiN
Interdiffusion zone
TiN
20 µm

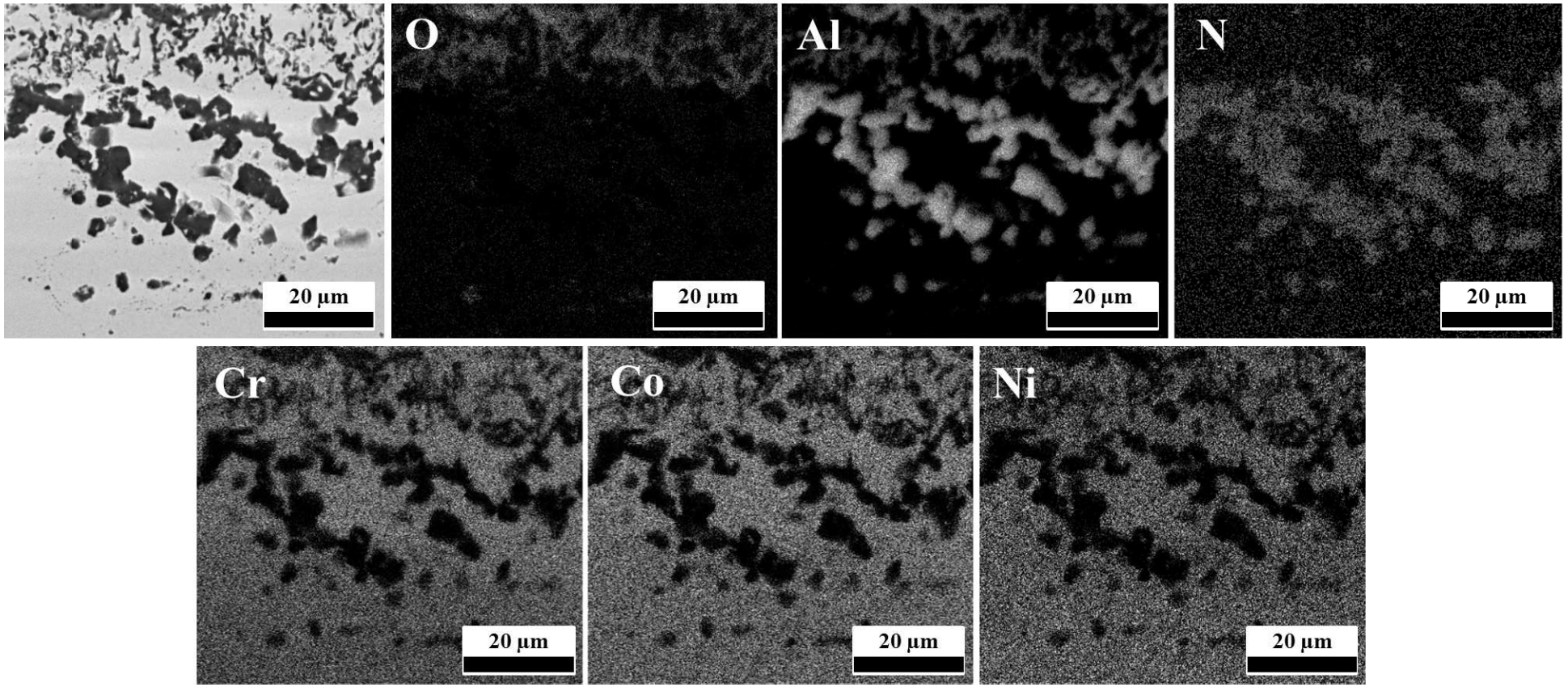
20 µm
O
20 µm
Al
20 µm
N
20 µm
Cr
20 µm
Co
20 µm
Ni
20 µm

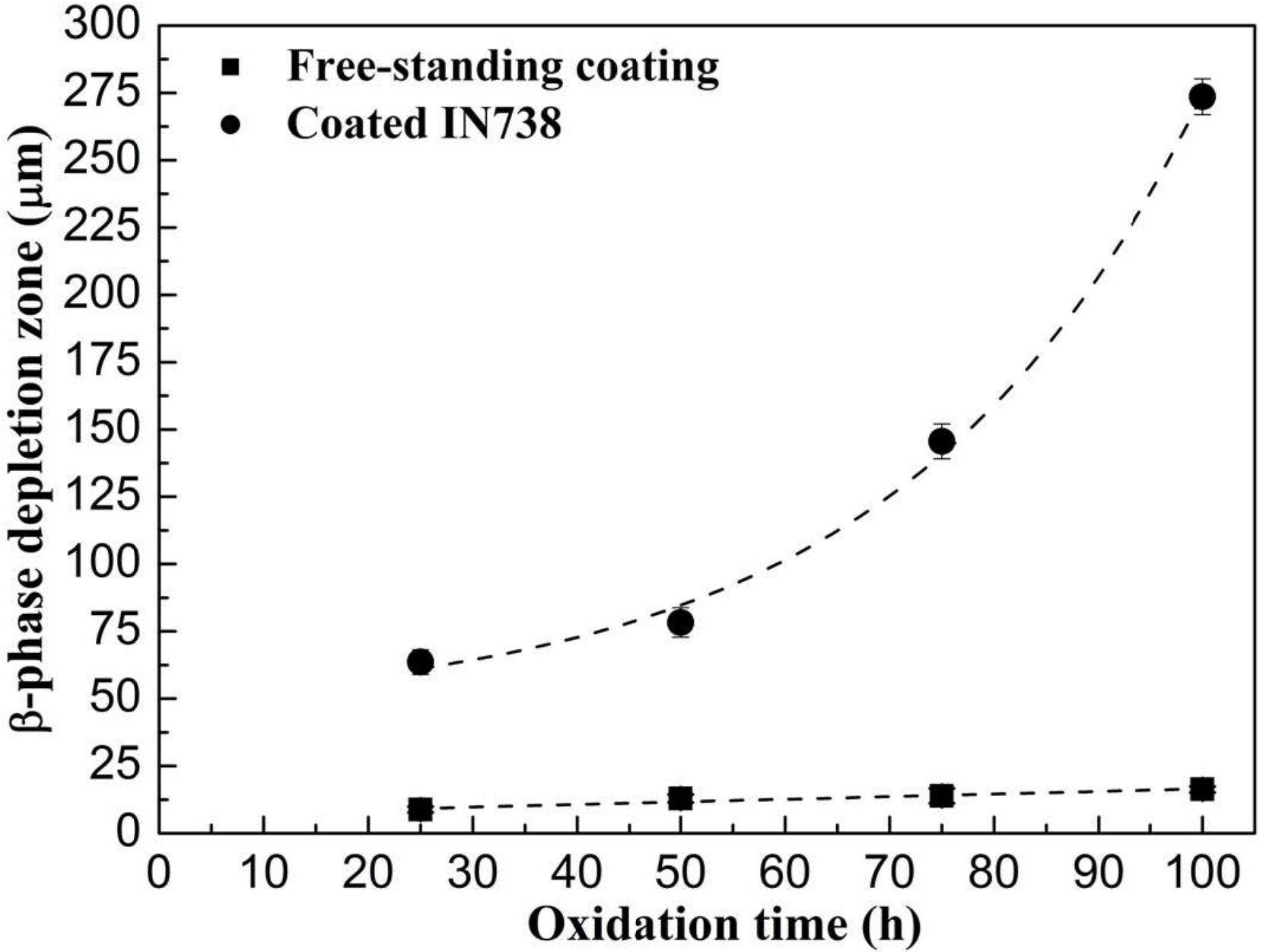
Free-standing coating
Coated IN738
β-phase depletion zone (μm)
Oxidation time (h)
0
25
50
75
100
125
150
175
200
225
250
275
300
0
10
20
30
40
50
60
70
80
90
100

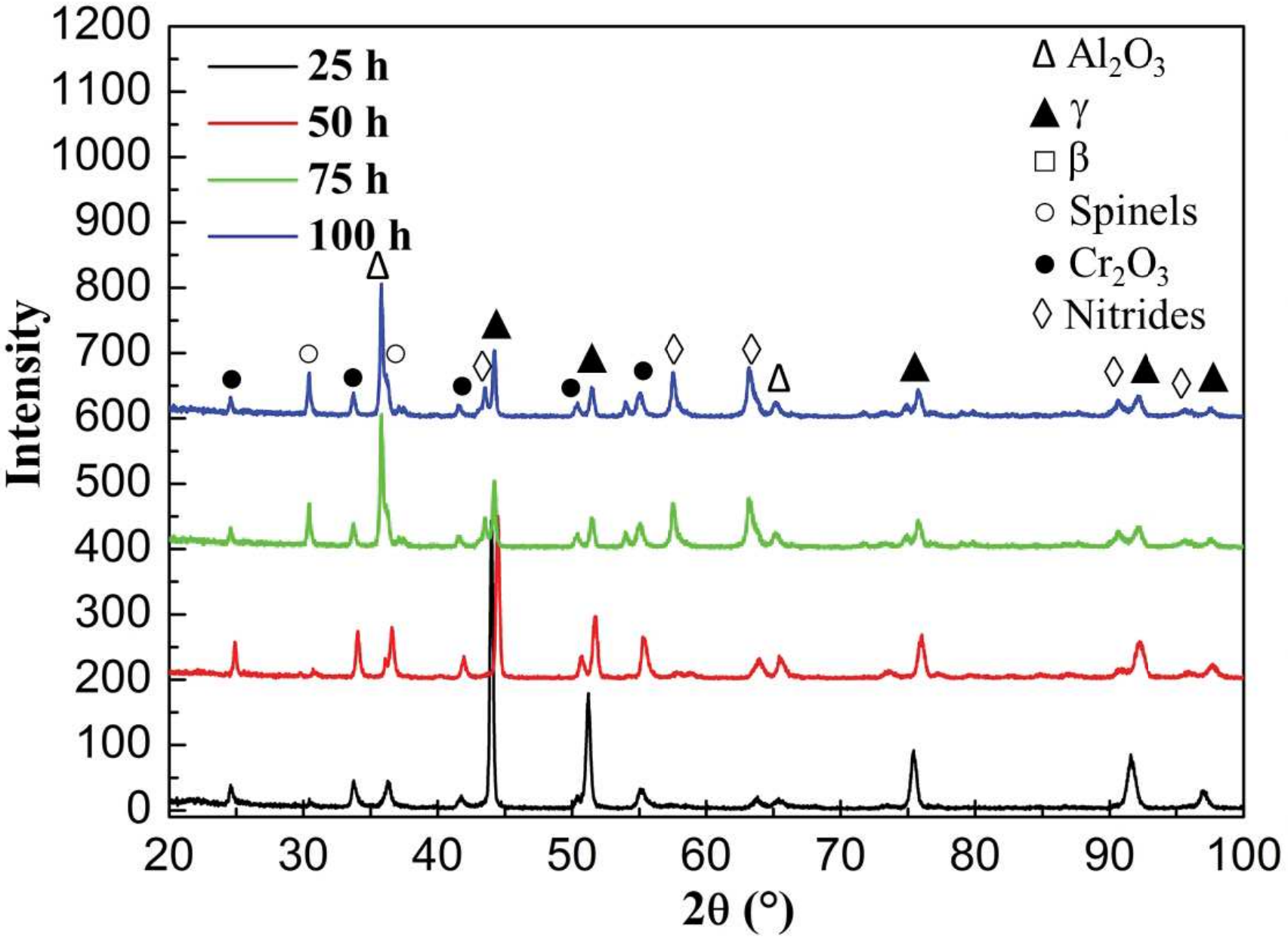
25 h
50 h
75 h
100 h
Δ Al2O3
▲ γ
□ β
○ Spinels
● Cr2O3
◊ Nitrides
Intensity
2θ (°)
0
100
200
300
400
500
600
700
800
900
1000
1100
1200
20
30
40
50
60
70
80
90
100

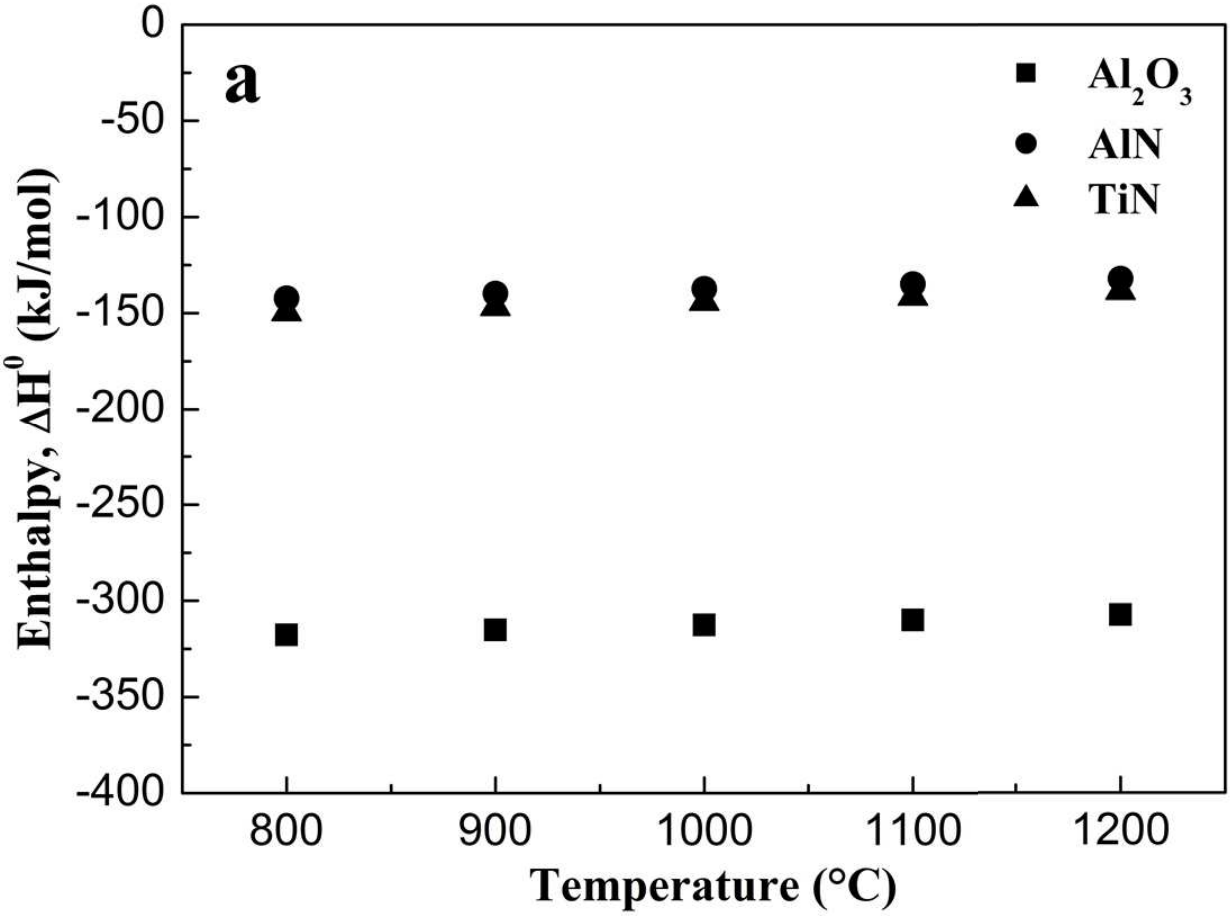
a
Al2O3
AlN
TiN
Enthalpy, ΔH0 (kJ/mol)
0
-50
-100
-150
-200
-250
-300
-350
-400
800
900
1000
1100
1200
Temperature (°C)

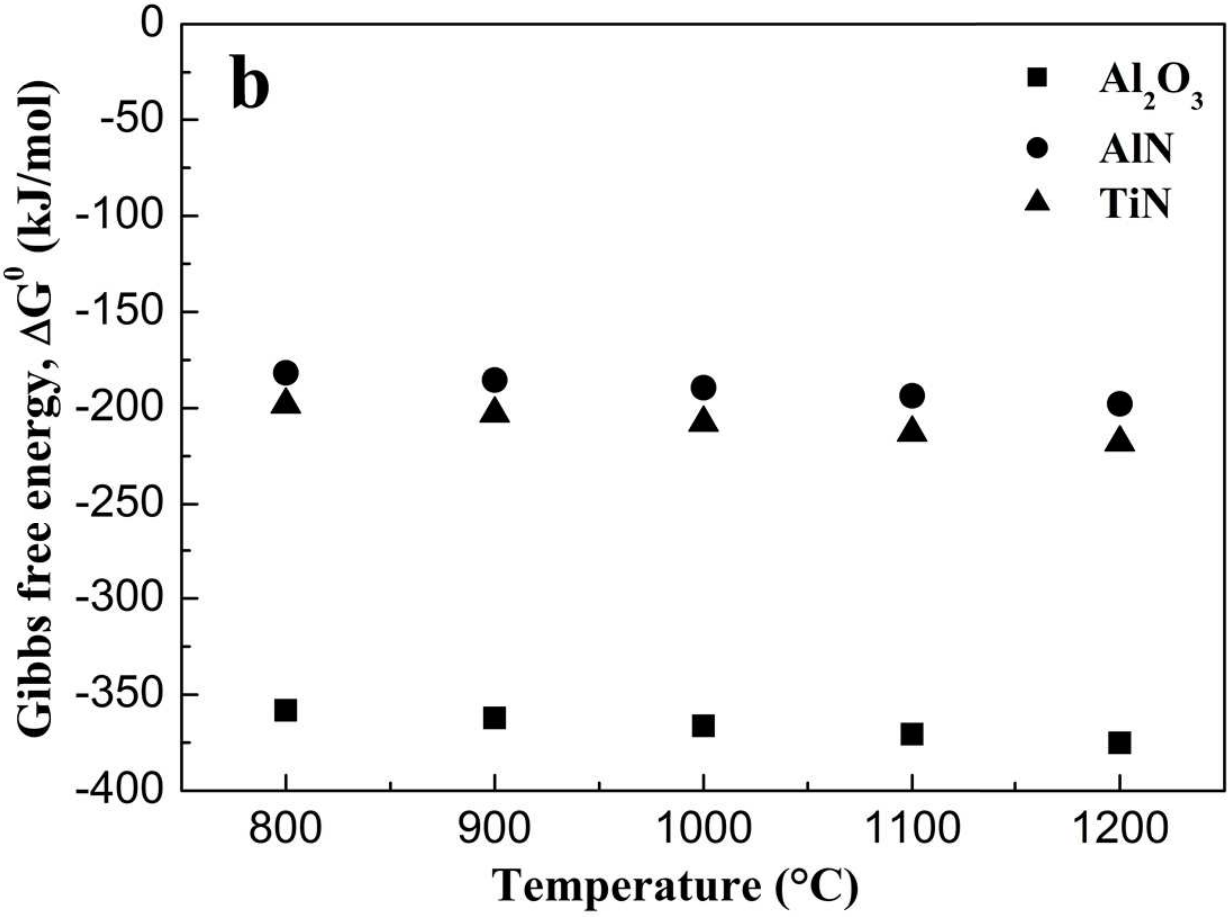
b
Al2O3
AlN
TiN
Gibbs free energy, ΔG0 (kJ/mol)
0
-50
-100
-150
-200
-250
-300
-350
-400
800
900
1000
1100
1200
Temperature (°C)

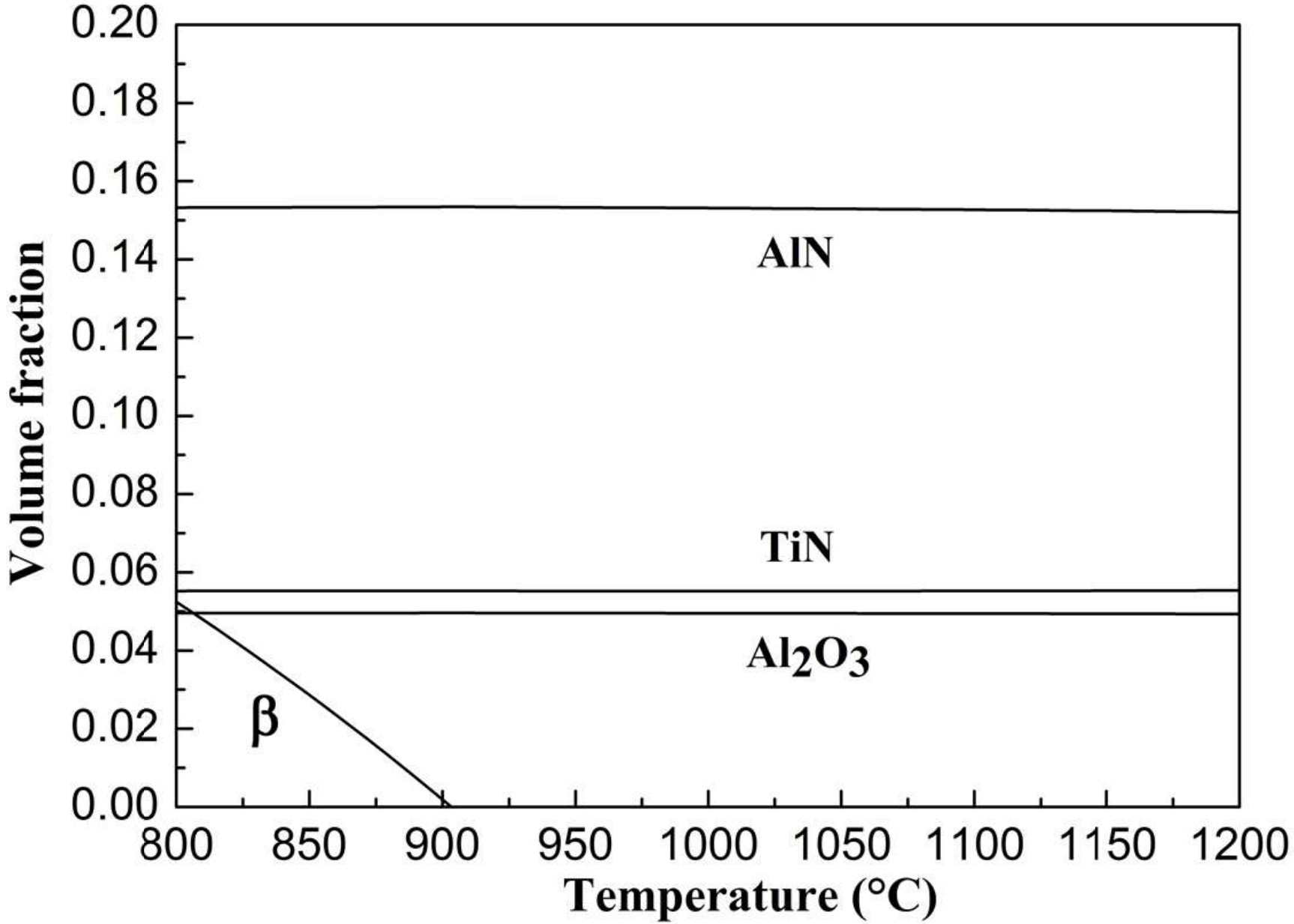
0.20
0.18
0.16
0.14
0.12
0.10
0.08
0.06
0.04
0.02
0.00
Volume fraction
AlN
TiN
Al2O3
β
800
850
900
950
1000
1050
1100
1150
1200
Temperature (°C)